DOI:10.1478/C1A0702001

Atti dell'Accademia Peloritana dei Pericolanti
Classe di Scienze Fisiche, Matematiche e Naturali
Vol. LXXXV, C1A0702001 (2007)
Adunanza del 28 novembre 2006

OPTICAL EMISSION SPECTROSCOPY STUDY OF THE EXPANSION DYNAMICS OF A LASER GENERATED PLASMA DURING THE DEPOSITION OF THIN FILMS BY LASER ABLATION

ENZA FAZIO, [a] FRANCESCO BARRECA, [a] BARBARA FAZIO, [b]
FORTUNATO NERI, [a]* AND SEBASTIANO TRUSSO [b]

(Nota presentata dal Socio Aggregato Fortunato Neri)

ABSTRACT. The dynamics of the expanding plasma produced by excimer laser ablation of different materials such as silicon, silicon carbide, graphite and tin powder were studied by means of time integrated, spatially resolved emission spectroscopy and fast photography imaging of the expanding plasma. Experiments were performed both in vacuum and in different pure background atmosphere (i.e. oxygen or nitrogen) and, finally, in gaseous mixtures (i.e. in O_2/Ar and N_2/Ar mixtures). These investigations were performed to gather information on the nature of the chemical species present in the plasma and on the occurrence of chemical reactions during the interaction between the plasma and the background gas. Then, we tried to correlate the plasma expansion dynamics to the structural and physical properties of the deposited materials. Experimental results clearly indicate that there is a strong correlation between the plasma expansion dynamics and the structural properties of the deposited thin films. In this respect, the investigations performed by means of fast photography and of optical emission spectroscopy revealed themselves as powerful tools for an efficient control of the deposition process itself.

1. Introduction

Pulsed Laser Deposition (PLD) is an experimentally simple and a very versatile method for growing thin films of a wide range of materials [1] with good crystalline quality. This possibility has generated an effort, with no precedents, in the study of the basic mechanism of PLD and of the plasma expansion dynamics produced by laser ablation of different material targets. The technique is based on the ablation process of a material induced by focusing a high energy pulsed laser on its surface. In spite of the simplicity of the experimental setup, the physical phenomena involved in the ablation process are very complex [2]. The involved mechanisms depend on the optical and structural properties of the target material and on the characteristics of the incident radiation such as the wavelength and the energy density. The stream of atoms, molecules and clusters that is ejected from the target surface during the ablation process, commonly known as "plume", rapidly expands, in vacuum or through a gas, towards the substrate surface. Although a lot of experimental and theoretical work has been done, many effects of the interaction of the laser beam with different targets in an ambient atmosphere are still not satisfactorily explained. It is known that,

being the plume composed of excited neutral and ionized species, it emits radiation that can be appropriately analyzed to obtain information about its composition and dynamics. In particular, by means of fast photography measurements, different regimes of the laser-induced plasma expansion dynamics have been evidenced. This information can be strictly correlated with the structural properties of the deposited thin films and can so give a very useful contribution to the comprehension and to the control of the deposition process itself.

Pulsed Laser Deposition is a good technique to grow SiO_x, SiC_xN_y, CN_x and SnO_x thin films because it permits to grow such materials without any contamination coming from reagent gases, as happens using the Chemical Vapor Deposition technique. In particular, by means of PLD in a controlled oxygen and/or O_2/Ar atmosphere, it is possible to prepare nearly stechiometric silicon dioxide thin films containing silicon nanostructures at relatively low temperatures, i.e. at temperatures compatible with the silicon integrated circuit technology [3].

In the present work we present both already published and new experimental data about the dynamics of laser pulse generated plasmas expanding in a background gas. The results are discussed in the framework of a general theory looking at the correlations between the plasma expansion dynamics and the structural properties of the deposited thin films. In particular we report about some optical emission spectroscopy and fast photography imaging studies of the plasma generated by the KrF excimer laser ablation of various materials such as silicon, silicon carbide, graphite and metal Sn, both in vacuum conditions and in presence of background gases. The experimentally determined behaviors are compared with the predictions of an analytical model which gives a complete description of the expansion of the plume and with some recent results reported in the literature. Evidences of the strong influence of the expansion plasma regime, not simply related to the overall reactive gases content, were found.

2. Theory

During PLD experiments the plasma generated from the target ablation is attenuated and thermalized by the gas environment, varying the film growth parameters such as the deposition rate and the kinetic energy distribution of the species. Furthermore some reactive gases can aid the formation of some molecules inside the plasma allowing the addition of the gaseous atomic species into the growing film. The raise of the background pressure generally leads to the following effects that depart from the free expansion behaviour: 1)an increase of the collisions on the expansion front with an increase of the fluorescence coming from all the species; 2) a sharpening of the plasma boundary that indicates the presence of a shock wave front; 3) a spatial confinement of the plasma due to a decrease of its velocity, determined by the repeated collisions with the gas molecules.

The plasma expansion in a gas environment has been described in the literature in terms of different phenomenological models depending on the experimental regimes, affected by the pressure range of the gas present during the deposition process, by the energy of the plasma species and by the temporal stage of propagation [4, 5, 6].

In vacuum, the plasma will expand in a way similar to a supersonic expansion with a free linear behaviour and a weak fluorescence will be visible, close to the target, due to collisions between the plasma species occurring just after the termination of the laser pulse.

At low pressure and in the early times of the expansion, the plasma dynamics is in good agreement with the drag-force model [2]. In this model the ejected species are regarded as an ensemble that experiences a viscous force proportional to its velocity V through the background gas:

$$V = V_0 e^{-\beta t} \tag{1}$$

or analogously

$$R = R_0(1 - e^{-\beta t}) \tag{2}$$

where R indicates the position of the front edge of the plasma, R_0 the distance at which the plasma propagation ceases (it is generally indicated as the stopping distance) and β a slowing coefficient. Both R_0 and β are phenomenological parameters whose values are, necessarily, determined by fitting the experimental data to Eq. (2). As reported in some works [4, 7], the estimated R_0 values are more than one order of magnitude larger than the calculated inelastic mean free path λ values. Such large differences are presumably due to the fact that R_0 is a rather complex function of several experimental parameters such as the background gas nature and pressure, the mass and the energy of the plasma and last, but not least, the (target material)/(gas specie) atomic mass ratio.

On increasing the ambient gas pressure, the viscous force increases, the expansion pressure inside the plasma drops and the backward pressure on the plasma towards the target increases. As a result, the expansion velocity decreases. The drag model holds only for low gas pressures; upon increasing the gas pressure values, this model predicts distances slightly shorter than those observed experimentally. Thus, the presence of a higher background gas pressure produces a non linear dependence on the distance from the target of the plasma front edge position. For high background pressures the plasma expansion follows the path described by the blast wave model [8, 9]. According to this model, created to describe the propagation of a shock wave through a background gas after an explosion, just after the arrival of the laser pulse on the target surface, a plasma ball develops and starts to expand along the normal to the target surface. The expanding plasma can act as a piston, compressing and accelerating the gas molecules to a supersonic velocity, with the formation of a shock wave ahead of the contact surface between the plasma and the ambient gas. The shock wave propagates away from the target and it is immediately followed by an expansion wave, which gradually reduces the shock strength. The presence of a foreign gas produces the plasma confinement and consequently an increase of the density of the ejected species in the plasma. This behaviour is consistent with a slowing down of the ejected species velocity both at large distances from the target and at high gas pressures. The position of the front edge, as a function of the time *t*, is given by the following relation:

$$R = \xi_0 (\frac{E}{\rho_0})^{1/5} t^{2/5} \tag{3}$$

where ξ_0 (≈ 1) is a factor related to both geometrical and thermodynamic quantities, E is the plasma energy and ρ_0 the density of the undisturbed gas. This model can strictly be applied only when the mass of the gas surrounding the shock wave is higher than the mass of the ablated material and only up to distances from the target at which the pressure

driving the moving front of the plasma is greater than the pressure of the gas at rest. Then the shock wave can be observed only in a limited spatial region R:

$$\left(\frac{3M_0}{4\pi\rho_0}\right)^{1/3} << R << \left(\frac{E}{P_0}\right)^{1/3} \tag{4}$$

where M_0 is the mass of the expanding plasma and P_0 is the pressure ahead of the shock wavefront [6, 8].

In the shocked region, the temperature raises reaching values of the order of several thousand of Kelvin degrees and producing an enhancement of the optical emission from the excited species in the plasma. The temperature values in this region can be obtained starting from the equation of state for a polytropic gas [10]:

$$T_s = \frac{2\gamma}{\gamma+1}\left[\frac{\gamma-1}{\gamma+1}M^2+1\right]T_0 \tag{5}$$

where γ is the specific heats ratio (≈ 1.2), *M* the Mach number and T_0 the temperature of the undisturbed gas. The Mach number can be evaluated from the *V=R/t* data, where *M=V/*v_s, *R* indicates the position of the shock wave moving front, and v_s is the sound velocity. In the same way it is possible to obtain the relation for the shocked region density ρ_s

$$\rho_s = \rho_0\frac{\gamma+1}{\gamma-1}. \tag{6}$$

In this region, the reached temperature values can influence the physical and chemical behaviors of the species. In reality, the chemical reactions can take place only if a sufficient mixing between the plasma and the gas species occurs. Such a mixing is governed by the diffusion processes across the contact surface between the plasma and the ambient gas. It reaches a sufficient extension if the gas diffusion range, evaluated in the shocked region, is comparable to the thickness of the shocked region itself. The gas diffusion range $D_r = \sqrt{4Dt}$ can be evaluated through the following diffusion coefficient relation:

$$D = D_0(T_s/T_0)^{0.75}(\rho_a/\rho_s) \tag{7}$$

where D_0 and ρ_a are the diffusion coefficient and the density of the ambient gas at atmospheric pressure and room temperature.

To sum up, the drag-force model predicts that the plasma could stop its propagation, because of the viscosity originating from collisions with the ambient gas species, while the blast wave model, that neglects the viscosity, predicts a continuous propagation as $R \propto t^{\frac{2}{5}}$. Experimentally the plasma generated in PLD experiments shows a behavior described by a mix of these two models: it starts following the drag model and then, when the viscous slowing of the plasma front edge coalesces to form the shock front, it will expand according to the blast wave model. In the last years, Arnold et al. [11] proposed an analytical approach to explain the complete dynamics of the laser generated plasma into ambient gas valid for any pressure value and for any spatial and temporal regime. This phenomenological model provides some differential equations for the characteristic radii

describing the spherical plasma expansion and takes into account three different process stages: an early stage where the plasma expansion is characterized by a free expansion with a linear behaviour ($R \propto t$); an intermediate stage where there is the shock wave formation and the plasma dynamics behaves as $R \propto t^{2/5}$; and a final stage where the plasma expansion stops. These regimes, that depend on the different process conditions, are also temporally unified so that a single analytical curve gives a complete description of the phenomenon.

Experimentally, the chemical nature of the background gas, its pressure and the plasma energy can determine the occurrence of one or more of these regimes and a family of R-t curves can be obtained. If these R-t experimental data are expressed in terms of the following dimensionless variables:

$$\widetilde{R} = R(\frac{2E}{P_0})^{-1/3}; \widetilde{t} = tv_s(\frac{2E}{P_0})^{-1/3} \tag{8}$$

where v_s is the sound velocity in the ambient gas, P_0 is the known pressure of the gas and E is the total energy of the plasma, then all of points will fall into a single curve. The energy of the plasma E depends on the coupling between the laser pulse and the target material and it is just a fraction of the laser energy.

In this work we adopt this latest approach to explain our results: we express all experimental data in dimensionless variables according to Arnold et al. [11] model.

Depending on the adopted experimental conditions all of the three stages, free expansion ($R \propto t$), shock wave formation ($R \propto t^{\frac{2}{5}}$) and the onset of the plume stopping were observed. Estimates of the plasma energy values were obtained from Eq. (3) applied to the R-t data in a limited range, *i.e.* where the ideal shock wave behaviour was observed. The influence, if any, of the gas on the laser-target coupling was neglected.

3. Experiments

The plasma, generated by a KrF excimer laser (wavelength 248 nm, pulse duration 25 ns, repetition rate 10Hz), and its expansion were studied by optical emission spectroscopy and fast photography imaging. Measurements were carried out in vacuum and also in the presence of both pure background and mixture gases. During the film deposition processes, the light emitted from the laser-induced plasma was collected at a right angle with respect to the plasma expansion direction. The collected light was transmitted by means of an optical fiber to the entrance slit of a 0.26m spectrometer (Lot-Oriel MS260i) equipped with an 1800 grooves/mm holographic grating. An intensified and gateable charge coupled device (Andor Technology iStar iCCD) with a variable gate was used as a detector (see Fig. 1).

The iCCD, placed at the spectrometer exit, was used to detect the optical emissions from the plasma and then to acquire the images of the expanding plasma. Taking into account the imaging properties of the optical system, a spatial resolution of about $1mm^2$ was estimated. For each experiment, by translating the optical system along the plasma expansion direction, light emission from the plasma was collected at different distances from the target surfaces. The acquisition of the spectra was synchronized with the laser pulse using the signal from a fast photodiode which collected a small portion of the incoming

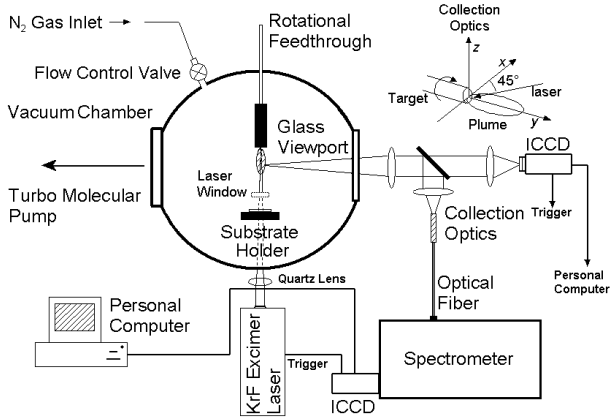

FIGURE 1. Optical emission spectroscopy experimental setup.

beam. A good signal to noise ratio has been obtained averaging each spectrum over several successive laser pulses and varying the intensification factor of the CCD as a function of the observation point with respect to the target surface. Moreover, normalization factors were experimentally determined, for each gate and intensification gate values, in order to correctly compare the acquired spectral intensities. Fast photography imaging of the expanding plasma was performed by using the same iCCD employed for the time integrated experiment; the images were recorded at different delay times after the laser pulse arrival.

In the following details of the experimental parameters adopted for the growth of the different materials investigated are reported.

SiC_xN_y -High purity (99.999%) reaction bonded polycrystalline SiC rod targets were ablated using an energy density of 7.0 J cm^{-2}. The experiments were performed in vacuum (residual pressure better than $1.33 \times 10^{-4)}$ Pa and in a high purity nitrogen gas atmosphere, varying the pressure between 2.6 and 133 Pa. In this case, the light generated from the plasma expansion was collected at distances d up to 15 mm away from the target surface. We adopted a gate width τ_G of 100 ms to get the time integrated spectra in a spectral range between 350 and 750 nm. For the time resolved measurements, the τ_G value ranged between 10 and 250 ns, depending on the experimental conditions. The images were collected with a gate width τ_G of 2 ns in the initial stage of the plasma expansion, then progressively increased up to 10 ns. Each image was averaged over 10 successive laser pulses.

SiO_x -A first set of SiO_x thin films was deposited in the presence of pure oxygen gas at pressure values up to 13.33 Pa while a second set was grown in an O_2/Ar gaseous mixture, keeping fixed the total pressure at 13.33 Pa and controlling the O_2/Ar ratio from 1/99 up to 80/20. The light emission from the plasma was collected at distances d up to 30 mm from the target surface. A gate width τ_G of 100 ms was set to get the time integrated spectra, while, for the time resolved measurements, a τ_G value between 10 and 250 ns, depending on the experimental conditions, was adopted. Fast photography imaging of the expanding plasma was performed at different delay times after the laser pulse arrival adopting a gate

width τ_G of 2 ns in the initial stage of the expansion and then progressively increasing it up to 100 ns.

CN_x - Carbon nitride thin films with different nitrogen concentration have been deposited by focusing the beam of a KrF excimer laser onto the surface of a graphite target. The films were grown both in pure nitrogen atmosphere at pressure of 1.3,13.3 and 66.7 Pa and in a mixed N_2/Ar atmosphere with a total pressure of 13.3 and 66.7 Pa and a N_2/Ar partial pressure ratio of 1/9 and 1/49, respectively. Light emission from the plasma was collected at distances *d* up to 30 mm from the target surface. A time gate of 100 ms was adopted for the time-integrated measurements. For the images acquisition, a time gate of 100 ns was adopted in the initial stage of the expansion and then progressively increased.

SnO_x - A set of SnO_x thin films, with a thickness of about 420 nm, were grown at the laser fluence of 1J/cm^2, at different deposition temperatures (in the range between RT and 800K), in vacuum and at different oxygen partial pressure values (from 0.13 Pa up to 66.7 Pa). The time integrated spectra were acquired in the 350-800 nm region at different distances from the target (from 1 up to 40 mm). In the same spectral region, we performed measurements of time resolved optical emission recorded at different distances from the target surface for all the chosen deposition conditions. At a given observation distance, optical time of fligth (TOF) spectra were obtained from the intensities of a selected emission as a function of the time delay. Fast photography images were collected both in vacuum and/or in oxygen atmosphere at different delay times (90, 200, 700 and 1750 ns) after the pulse arrival.

Structural characterization of the films was performed by means of micro-Raman scattering, infrared transmission and X-ray photoelectron spectroscopies; for experimental details we refer to the following references [3, 12].

4. Results and Discussion

During the ablation process of a SiC target in a nitrogen atmosphere, we tried to better identify the precursor processes which take place during the plume expansion and we focused our attention on the chemical reactions occurring in the plasma in order to investigate the influence of the nitrogen gas pressure on the incidental CN or SiN species formation. Subsequently, we investigated about the presence of CN molecular species in the plasma obtained by ablating a graphite target both in pure nitrogen atmosphere and in a $\mathrm{N_2/Ar}$ gaseous mixture, trying to elucidate the role played by the ambient gas on the CN formation mechanism.

The same approach has been followed to grow SiO_x thin films. The films were grown in pure oxygen and in a mixed $\mathrm{O_2/Ar}$ atmosphere. In this case, the aim of our study is to show the influence of the dynamics of the expansion plasma on the growth of such kind of thin films when a well definite compositional parameter x is required. In fact, as shown in a previous paper, this requirement is mandatory to observe silicon nanocrystal formation in a SiO_x matrix [3].

Then, we tried to find a clear correlation between the plasma expansion dynamics and the stoichiometry and the structural properties of CN_x thin films, grown in pure nitrogen and in a mixed $\mathrm{N_2/Ar}$ atmosphere. In particular, we analyse the influence of the gas composition and pressure on both the nitrogen content and the sp^2 carbon clustering process.

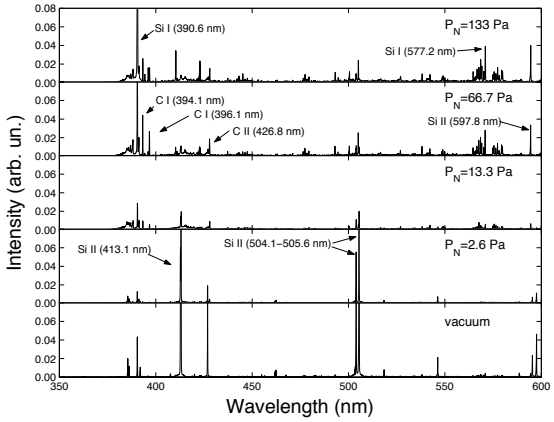

FIGURE 2. Time integrated optical emission spectra acquired at d=10 mm from the target in vacuum and at different nitrogen pressures. *With permission from reference* [13]

SiC_xN_y - We performed time integrated spectroscopy measurements to identify the species present in the plasma. The emission spectra, acquired at a distance $d = 10mm$ from the target in vacuum and in nitrogen atmosphere at different pressures, are characterized by the typical emission lines of silicon and carbon species (Si I, Si II, C I, C II) both neutral and singly ionized (see Fig. 2). For comparison in Table 1 are reported the most relevant emissions observed together with the corresponding electronic transitions. If we consider the intensity of the typical emission lines as a function of the distance from the target, two different behaviours can be observed increasing P_N. For pressure values up to 2.6 Pa, the intensities of all of the emissions decrease as the distance from the target surface increases (see Fig. 3). A slight decrease of the emission is also observed as the nitrogen pressure is raised. For higher P_N values, from 13.3 Pa up to 133.3 Pa, the emission lines show a clear secondary maximum at a definite distance from the target surface, with the notably exception of the C II related one. Beside the atomic emissions, two molecular bands are visible even at the lowest nitrogen pressure and their intensities increase with P_N. These two bands were identified as due to the vibrational sequences of the CN molecule violet system ($B^2\Sigma^+ \rightarrow X^2\Sigma^+$) with band head at 388.3 nm ($\Delta\nu = 0$) and 421.6 nm ($\Delta\nu = -1$) [14]. In Fig. 4 is reported the spectral region where the substructure of these bands is readily observable.

The intensity of the CN band head emission at 388.3 nm as a function of the observation distance d from the target is at variance with that exhibited by the atomic emission lines, as shown in Fig. 5. In particular, the emission intensity is low near the target and reaches its maximum value at the distance d of $5\ \mathrm{mm}$. On the contrary, atomic emissions for $P_N \leq$ 13.3 Pa are strongest near the target surface and decrease moving away from the target. The position of such a maximum is shifted toward the target surface for higher pressure values.

TABLE 1. Emitter specie, wavelength, electronic transition and upper level energy for some of the most intense observed emission lines.

Specie	Wavelength (nm)	Transition	E_k (eV)
Si II	385.6	$4p\ ^2P^0_{3/2} \rightarrow 3p^2\ ^2D_{5/2}$	10.07
Si I	390.6	$4s\ ^1P^0_1 \rightarrow 3p^2\ ^1S_0$	5.08
C I	394.1	$6p\ ^1S_0 \rightarrow 3s\ ^1P^0_1$	10.83
C I	396.1	$6p\ ^1D_2 \rightarrow 3s\ ^1P^0_1$	10.81
Si II	413.1	$4f\ ^2F^0_{7/2} \rightarrow 3d\ ^2D_{5/2}$	12.84
C II	426.8	$4f\ ^2F^0_{7/2} \rightarrow 3d\ ^2D_{5/2}$	20.95
Si II	504.1	$4d\ ^2D_{5/2} \rightarrow 4p\ ^2P^0_{1/2}$	12.53
Si II	505.6	$4d\ ^2D_{5/2} \rightarrow 4p\ ^2P^0_{3/2}$	12.53
Si I	577.2	$5p\ ^1S_0 \rightarrow 4s\ ^1P^0_1$	7.23
Si II	597.8	$5s\ ^2S_{1/2} \rightarrow 4p\ ^2P^0_{3/2}$	12.15

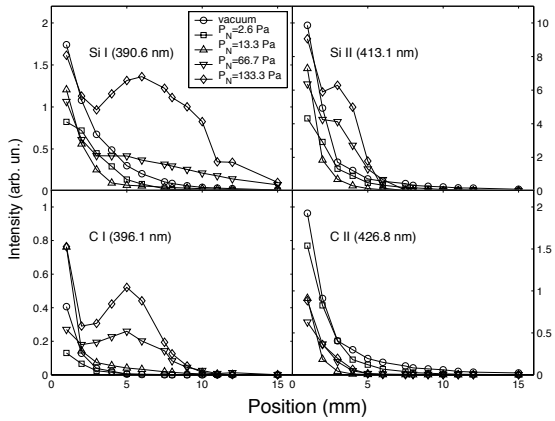

FIGURE 3. Intensity of SiI, Si II, CI and C II emissions as a function of the observation distance from the target, for different nitrogen pressures. *With permission from reference* [13]

This behaviour is attributed to the cooling and the recombination processes which occur just after the termination of the laser pulse. Near the target surface, at the early stage of the plasma formation, the density of the free electrons and of the emitting species (both neutral and singly ionized) is higher and the collisions favour the excitation processes. During the plasma expansion, its density drops as well as the probability that each species gets excited. For nitrogen pressures higher than 13.3 Pa, the plasma interaction with the ambient gas

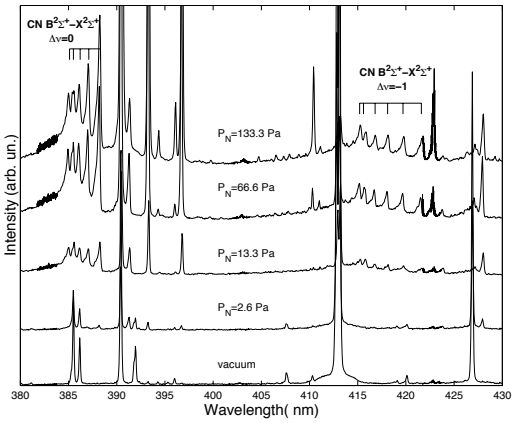

FIGURE 4. Expanded view of the 380-430nm spectral region of the emission spectra shown in Fig. 2. *With permission from reference* [13]

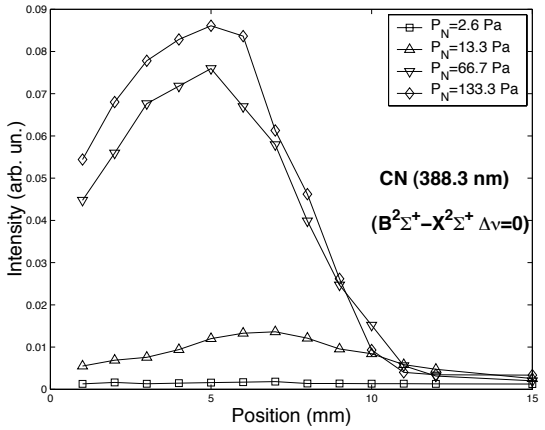

FIGURE 5. Intensity of the CN band head emission at 388.3nm as a function of the observation distance from the target, for different nitrogen pressures. *With permission from reference* [13]

becomes prominent leading to the observed maximum in the atomic line intensities. This behaviour is a clear evidence of the CN molecule formation.

Other experiments performed ablating a graphite target in the presence of nitrogen have already shown the emission from CN complexes [14, 15, 16, 17, 18, 19, 20] and from C_2 species belonging to the Swan system (d $^3\Pi_g \rightarrow$ a $^3\Pi_u$, $\Delta\nu$ = 2, 1, 0). Generally, it is supposed [14, 16, 19, 21] that CN molecule formation in the gas phase occurs through the

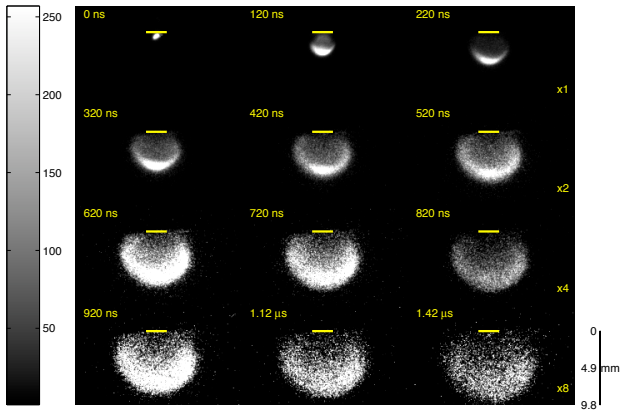

FIGURE 6. CCD images of the emission from the plasma recorded at a nitrogen partial pressure of 66.7 Pa. *With permission from reference* [13].

reaction:

$$C_2 + N_2 \rightleftharpoons 2CN \tag{9}$$

In our case, ablating SiC target in presence of nitrogen, we have no evidence of C_2 species emissions in any of the adopted experimental conditions. So, we supposed that their concentration in the plasma should be very low, if indeed any at all. The following reaction needs to be considered:

$$C + N_2 \rightleftharpoons CN + N + \Delta E, \tag{10}$$

where ΔE is the enthalpy of the reaction itself. We consider the binding energy value of the C-N bonds, the dissociation energy of N_2 and the ΔE value for the above reaction that turns out to be -2.01eV. Nitrogen molecules can be dissociated by means of electron-molecule collisions, a mechanism that should be more efficient near the target surface where both electron density and temperature are very high [22, 23]. Nevertheless, the CN molecules, eventually formed near the target surface, could be easily dissociated as well. Then, to explain the occurrence of a maximum in the CN line emission intensities at nitrogen pressure above 2.6 Pa, it is required the presence of an alternative mechanism, able to deliver sufficient energy to allow for the reaction (10). This mechanism is the formation of a shock wave as a consequence of the interaction of the expanding plasma and the background gas. In order to check for the presence of the shock wave, we performed fast photography imaging of the expanding plasma at different nitrogen pressures.

In Fig. 6 are shown CCD images of the emission from the plasma recorded at a nitrogen partial pressure of 66.7 Pa. A bright edge in coincidence with the contact surface between the plasma and the ambient gas can be clearly observed indicating a confinement of the plasma. From the images it was possible to evaluate the distance from the target surface R at which the maximum of the intensity occurs as a function of time. The variation of the position of the plume front edge as a function of time for different nitrogen pressures is shown in Fig. 7a. It is evident that for $P_N \leq 2.6$ Pa the plasma shows a free expansion

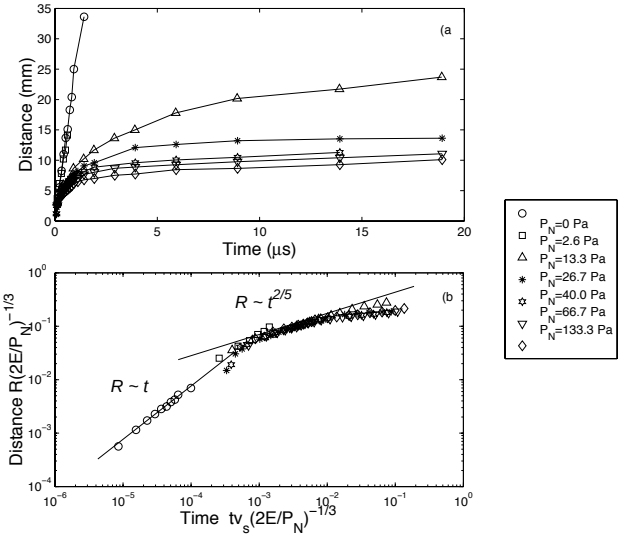

FIGURE 7. a) Variation of the position R of the plasma front edge as a function of the time for different P_N values. b) The same data of (a) in terms of the dimensionless variables $\tilde{R}$ and $\tilde{t}$ (see text). *With permission from reference* [13]

dynamics while for higher pressures it slows down. Such a slowing down is more and more effective as the pressure is raised. The same experimental data $R - t$ are expressed in terms of dimensionless variables according to the analytical model proposed by Arnold et al.. The corresponding plot of the distance vs time, in dimensionless variables, is shown in Fig. 7b.

It is important to outline that while the P_0 value is known, being an experimental parameter, the energy of the plasma E should be determined. In order to make such an estimate, we carried out a fitting procedure with equation (3) only for those $R-t$ data that showed an almost linear behaviour when plotted as R^5 vs t^2. The obtained E values ranged between 4 and 6 mJ. Taking into account that the laser pulse energy was 25 mJ, we concluded that about 20% of the laser energy has been transferred to the plasma.

From Fig. 7b we observed that all the R-t data collapse onto a single curve. Moreover, it is evident that in the initial stage the expansion follows a free expansion behaviour law ($\tilde{R} \propto \tilde{t}$), then the expansion behaves as predicted by eq. (3) ($\tilde{R} \propto \tilde{t}^{2/5}$). In the late stage a further slowing down is evident indicating the onset of the plasma stopping. From the fast photography measurements the formation of a shock wave is evident for $P_N \geq$ 13.3 Pa. Moreover, it has been observed that the T_s values obtained from the relation (5) in the temporal region where the shock wave behaviour holds ($10^{-4} \leq \tilde{t} \leq 10^{-2}$) decrease from 10^5 K down to 10^4 K. Such temperature values are high enough to produce physical and chemical changes of the species in the shocked region. At a distance d=5 mm and a pressure P_N=133.3 Pa, $i.e.$, values at which the maximum intensity of the CN emission occurred in the time integrated spectroscopy measurements, a value of about 250

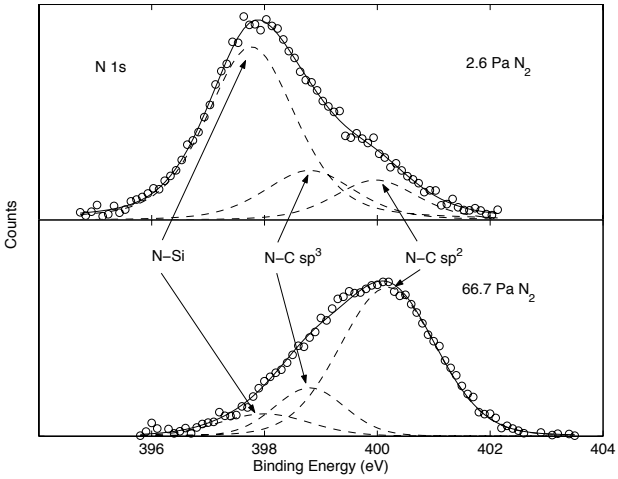

FIGURE 8. a) X-ray photoemission spectra from N1s level. *With permission from reference* [13]

μm for the diffusion range $D_r = \sqrt{4Dt}$ is obtained from the relation (7) where D_0=0.182 cm^2s^{-1}. This value is comparable to the corresponding thickness of the shocked region Δ=150 μm evaluated from the relation $\Delta = \frac{R}{3}(\gamma - 1)/(\gamma + 1)$ [9]. Thus, a sufficient mixing exists between the plasma species and nitrogen in the shocked region to allow the chemical reactions for the production of CN species on the basis of the reaction (10).

In order to obtain information about the stoichiometry and the bonding configuration present in the growing films, X-ray Photoemission Spectroscopy (XPS) measurements were performed on the samples grown at P_N=2.6 Pa and P_N=66.7 Pa. In Fig. 8 are shown the N1s core level photoemission spectroscopy data. The data were fitted, according to the literature attributions, with a three subbands model, supposing the presence of N-Si, N-C sp^3 and N-C sp^2 bonds. A substantial modification of the chemical bonding environment in the films has been observed varying the nitrogen partial pressure. It is clear from the analysis of the fitting results the prevalence of the silicon coordinated nitrogen bonds at low pressures while, increasing the nitrogen partial pressure, an almost exclusively carbon coordination is dominant.

CN_x -Time integrated optical emission spectroscopy measurements have been performed to gather information on the nature of the chemical species present in the plasma. The spectra, shown in Fig. 9, have been acquired at a distance d of 5mm from the target and at different nitrogen partial pressures. They are characterized by two emission bands at 388 nm and 516 nm. The observed emission lines are due to the vibrational sequences of the CN molecule violet system ($B^2\Sigma^+ \rightarrow X^2\Sigma^+$,$\Delta\nu = 0$), and to the vibrational sequences of the C_2 molecular specie ($d^3\Pi_g \rightarrow a^3\Pi_u$,$\Delta\nu = 0$), respectively.

In particular, in Fig. 10a,b are shown the intensities of the CN and C_2 band head emissions as a function of the observation distance from the target at different pure nitrogen partial pressure. The evolution of the emission lines shows that increasing the nitrogen partial pressure, the intensity of CN related emission increases and its maximum position

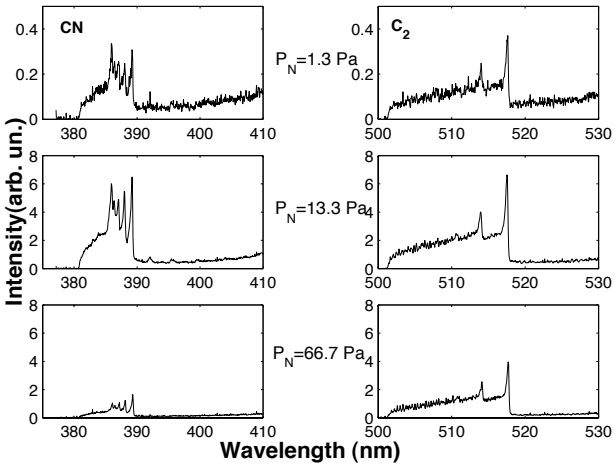

FIGURE 9. a) Time integrated optical emission spectra of the CN and C_2 species, acquired at 5 mm from the target and at different nitrogen partial pressures. *With permission from reference* [12]

remains unchanged. Nevertheless, reaching the value of 66.7Pa, the intensity of the CN emission decreases and, at the same time, the maximum shifts towards the target surface. About the C_2 molecules emission, it is evident that its intensity decreases with d and its maximum value is always located near the target.

Time integrated optical emission spectroscopy measurements have also been performed in presence of N_2/Ar mixed atmosphere at the total pressure of 13.3 and 66.7Pa with N_2/Ar partial pressure ratios of 1/9 and 1/49, respectively. From Fig. 10c and d, it is evident a different behavior of the CN and C_2 molecules related emission in presence of N_2/Ar gaseous mixture with respect to the one observed in pure N_2 atmosphere. The peak intensity emission from CN species is nearly constant while the C_2 emission increases with the total pressure up to 66.7 Pa. Moreover at the highest pressure value, the emission maxima shift towards the target for both the species.

Concerning the plasma expansion dynamics three different regimes were identified: free expansion, shock wave formation and plasma stopping depending on the experimental conditions adopted. In Fig. 11 the variation of the position R of the plasma front edge as a function of time is reported. This trend is obtained from the time resolved images of the expanding plasma, not shown here, and refers to the expansion in different pure nitrogen pressure and in mixed N_2/Ar atmosphere. As can be seen the expansion is weakly influenced by the presence of the gas at the nitrogen partial pressure of 1.3 Pa. In this case, in fact, the dynamics of the expanding plasma follows a linear behavior. At longer delay times and increasing the nitrogen pressure, interaction with the gas becomes more and more effective; as a conseguence, a slowing down and finally the stop of the expansion occurs. The trend of the expansion plasma in the N_2/Ar gaseous mixture is very similar to the one shown in pure nitrogen atmosphere. Nevertheless, in this case, shock wave and plasma stopping were observed also at lower gas pressure values with respect to the pure

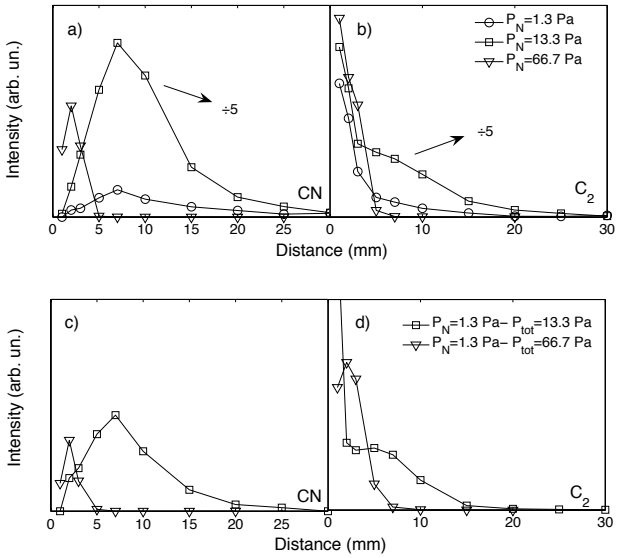

FIGURE 10. a) Intensity of the CN and C_2 band head emission as a function of the observation distance from the target at different pure nitrogen partial pressure and at different N_2/Ar mixture partial pressure. *With permission from reference* [25]

N_2 one. In particular, the expansion dynamics in the 13.3 Pa of N_2/Ar can be compared to the one observed in 66.7Pa of pure N_2. It has been observed that the shock wave regime and the stopping of the plasma are present for all the mixtures, thus argon atoms are more effective than nitrogen molecules in limiting the expansion of the plasma.

Looking for a correlation between the stoichiometry and the structural properties of the growing CN_x films and plasma expansion dynamics, X-ray photoelectron spectroscopy (XPS) and visible micro-Raman measurements were performed. In particular, from the ratio of the C 1s and N 1s photoelectron peak intensities, each multiplied by an appropriate sensitivity factor, the compositional parameter x has been estimated. Concerning the samples grown in pure nitrogen atmosphere, the nitrogen content x increases from 0.27 at P_N=1.33Pa up to 0.32 upon increasing the nitrogen partial pressure up to 13.3 Pa, but when it the latter is raised to 66.7 Pa, x value decreases to about 0.17.

Visible Raman spectroscopy was performed to obtain information about the structure of the growing films, being this technique sensitive to the sp^2 carbon phase and indirectly probing the evolution of the sp^3 one. Generally, Raman spectra of a carbon like system is characterized by two contributions, the so called D and G bands, respectively related to the motion of the sp^2 carbon atoms and to the breathing mode of the aromatic rings. In our case, the trend of the structural properties, as evaluated from the I_D/I_G ratio, shows that increasing the nitrogen partial pressure from 1.3 up to 66.7 Pa, a sp^2 carbon clustering process is favoured (see Table 2) even if the nitrogen content in the films decreases.

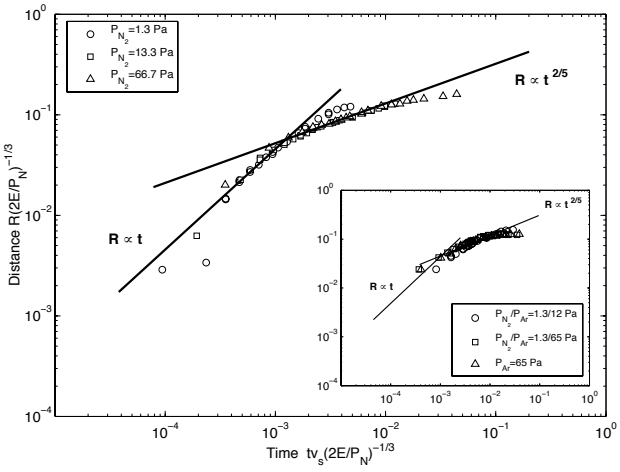

FIGURE 11. a) Plot of the distance vs time in dimensionless variable for pure nitrogen atmosphere and for nitrogen/argon gaseous mixture case (inset). *With permission from reference* [24]

This behaviour is explained in terms of a reduction of the kinetic energy of the depositing species reaching the substrate and, thus, is related to the change of plasma expansion dynamics from linear behaviour to shock wave formation, followed by the stopping of the plasma.

TABLE 2. Deposition conditions and summary of parameters deduced from XPS and Raman measurements.

Sample	F(J/cm^2)	P_N/P_A(Pa)	x	I_D/I_G
N1	1.4	1.3/-	0.27	0.33
N2	1.4	13.3/-	0.32	0.48
N3	1.4	66.7/-	0.16	0.57
NA1	1.4	1.3/12.0	0.09	0.32
NA2	1.4	1.3/65.4	0.03	0.30

In the two samples grown in a N_2/Ar mixed atmosphere, the nitrogen content drops from 0.27 down to 0.03, even if the nitrogen partial pressure was kept fixed. A further evidence is that the nitrogen content of the samples grown in the gaseous mixture is as low as that of the sample deposited at 1.33 Pa in pure nitrogen gas. Also the I_D/I_G ratios remain almost constant and comparable to the lowest one. On the contrary we should have expected to observe higher values, considering the total pressure at which the deposition took place. This is further evidence of the strong influence of the dynamics of the expansion plasma

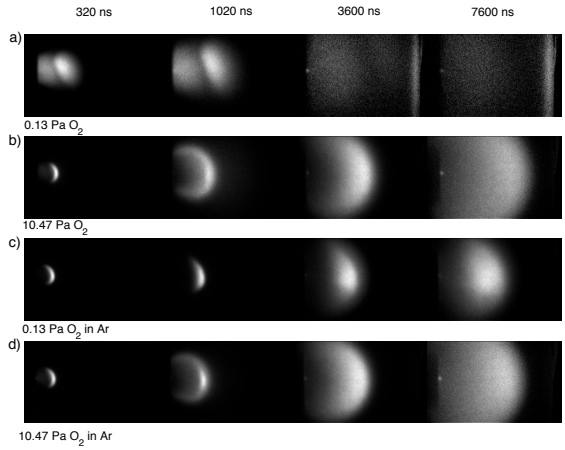

FIGURE 12. a) CCD image of the emission of the expanding plasma for different time delay under different experimental conditions (see text). *With permission from reference* [26]

regime, rather than the total pressure value, on the stoichiometry and the structure of laser ablation deposited carbon-nitrogen thin films.

SiO_x - Fast photography investigation of the dynamics of the expansion plasma, produced by excimer laser ablation of a silicon target in both an oxygen and a mixed O_2/Ar atmosphere, was carried out. In Fig. 12 are reported spots of the expanding plasma in a pure controlled oxygen atmosphere at 0.13 and 10.47 Pa.

At low pressure the plasma starts to decompose in two well distinct regions: the first one shows a nearly spherical expansion, the second one moves faster and can be observed at a different delay time with respect to the arrival of the laser pulse. Upon increasing the oxygen gas pressure, a deviation from the linear behaviour has been observed followed by the formation and the development of a shock wave. The occurrence of the shock wave is indicated by the presence of a bright edge in correspondence of the contact surface between the expanding plasma and the ambient gas at rest.

In the mixed O_2/Ar atmosphere, in spite of what observed in pure oxygen gas, there is no evidence for a linear behaviour while the formation of a shock wave is clearly evident for all the mixtures (see Fig. 12).

In Fig. 13 is shown the plot of the distance vs time in dimensionless variables.

It is evident that the expansion in pure oxygen gas shows two distinct slopes as a function of $\widetilde{t}$: a linear behaviour typical of a free expansion regime (R $\propto$ t) followed by a region where the relation $R \propto t^{2/5}$ holds. The linear behaviour holds for ambient pressure up to 2.67 Pa while, at higher oxygen pressure, the shock wave develops. In the case of O_2/Ar gaseous mixture, as evidenced from the plot of the *R-t* experimental data shown in the inset of the Fig. 13, only the shock wave regime is present for all the mixtures.

The development of the shock wave induces an increase of the shocked region temperature, with values ranging between $10^4 \div 10^5$ K. The temperature increase is supposed to

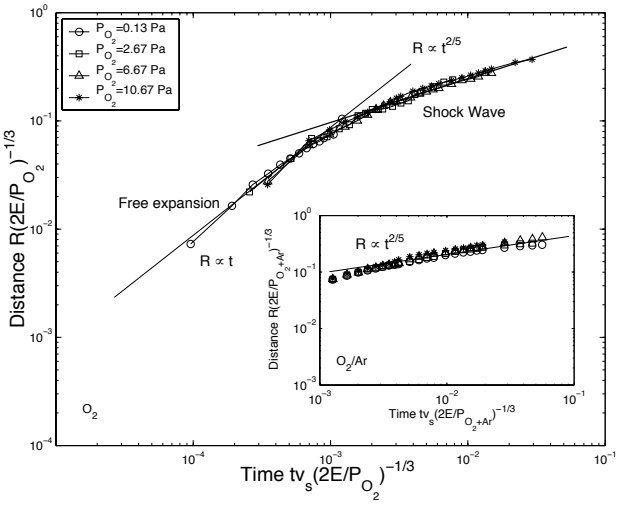

FIGURE 13. a) Plot of the distance vs time in dimensionless variables at different oxygen partial pressure. In the inset the same plot is reported for the O_2/Ar gaseous mixture case. *With permission from reference* [26]

enhance the dissociation of oxygen molecules by increasing the efficiency of the silicon oxidation reaction:

$$Si + O_2 \rightarrow SiO + O + \Delta E \tag{11}$$

Taking into account that the dissociation energy of an oxygen molecule is 5.2 eV, while the binding energy of SiO is 7.4 eV, the reaction Eq. (12) is exothermic with ΔE=2.2 eV. Generally, collisions between the species present in the plasma and oxygen molecules can lead to SiO formation. This process is favoured as the density of oxygen molecules increases. As a consequence, the films grown at the highest oxygen pressure (10.67 Pa) show a nearly stoichiometric composition due to an increased efficiency of the oxidation reaction under high pressure conditions. Nevertheless, also the films grown in the presence of an O_2/Ar gas mixture even with an oxygen partial pressure values as low as 0.13 Pa, show compositional parameter values around 2.0.

The most plasible explanation is that the shock wave development determines an increase of the temperature in the shocked region that produces an increase of the rate of Eq. (12). As a consequence, films with a compositional parameter *x* of about 2 have been grown in presence of the shock wave, irrespective of the oxygen content in the gaseous mixture (see table 3). Then, we can conclude that the total pressure, rather than the content of the reactive oxygen gas at which the deposition takes place, influences the plasma expansion dynamics, having a strong effect on determining the stoichiometry and the structural properties of the films.

TABLE 3. Deposition conditions and the compositional parameters x obtained from FTIR analysis for the samples deposited in pure O_2 and mixed O_2/Ar atmosphere.

Sample	P_{O_2}(Pa)	P_{O_2}/P_A (Pa)	x
A1	0.13	–	1.20
A2	2.6	–	1.65
A3	6.5	–	1.98
A4	10.4	–	2.01
B1	–	1/99	1.98
B2	–	20/80	1.95
B3	–	50/50	2.01
B4	–	80/20	2.02

SnO_x - SnO_x thin films were grown as reported in the experimental section. Information about their atomic composition and bonding configurations were obtained by means of XPS spectroscopy.

TABLE 4. Deposition conditions and compositional parameters x obtained from XPS measurements for all the grown SnO_x thin films.

Sample	F(J/cm^2)	T_d(K)	P_{O_2} (Pa)	x
S004	1	300	–	1.22
S006	1	570	–	1.59
S003	1	770	–	1.85
S005	1	970	–	1.63
S007	1	470	0.13	1.30
S008	1	520	0.13	1.64
S010	1	570	0.13	1.74
S012	1	470	1.3	1.67
S014	1	470	13.3	2.14
S011	1	470	66.7	1.45

The results show that the compositional parameter x varies as a function of the deposition parameters (temperature and pressure). In particular, x increases from 1.22 up to 1.85 for the samples grown in vacuum upon increasing the deposition temperature from 300K up to 770K (see Table 4); i.e. the films are sub-stoichiometric with respect to tin dioxide and the substrate temperature plays a crucial role allowing an increasing oxygen incorporation. In Fig. 14 FTIR absorption spectra of the samples grown in vacuum (a), in presence of

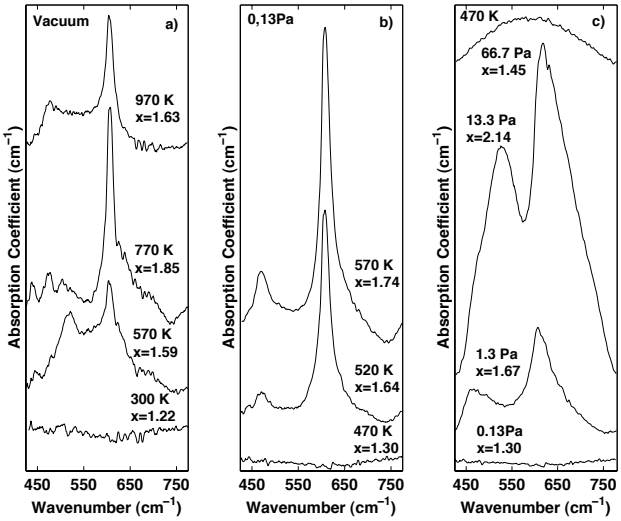

FIGURE 14. FTIR absorption spectra of the samples grown in vacuum (a), in presence of 0.13 Pa of P_{O2} as a function of the temperature (b) and at 470K as a function of P_{O2} (c).

0.13 Pa of P_{O2} as a function of the temperature (b) and at 470K as a function of P_{O2} (c), respectively are shown.

Concerning the sample grown in vacuum at RT, there is no evidence of the absorption bands related to the Sn-O bonds. Upon increasing T_d two bands, attributed to Sn-O and O-Sn-O stretching modes, become evident at around 490 and 610 cm^{-1}. The evolution of FTIR spectra (see Fig. 14a) and of the estimated x values as a function of T_d indicates that the deposition process performed in vacuum is unable to produce a congruent transfer process. At the same time there is evidence that the increase of the deposition temperature plays a crucial role in the incorporation of oxygen atoms in the samples. Nevertheless, also at the highest temperature adopted, the sample results sub-stoichiometric (x=1.85 at T_d=770 K).

In order to increase the oxygen content, a second set of SnO_x thin films were grown at P_{O2}=0.13 Pa and at temperatures values of 470, 520 and 570 K, i.e. keeping the deposition temperature relatively low. The compositional parameter x increases from 1.3 up to 1.74 upon increasing T_d. It is worth noticing that the x value of 1.74 relative to the sample grown at P_{O2}=0.13 Pa and T_d=570 K is comparable to the values of 1.85 and 1.63 of the samples grown in vacuum at 970 and 770 K, respectively. FTIR spectra confirmed that also the structural properties evolve in a similar way. Upon increasing T_d up to 570 K, in fact, the absorption bands related to Sn-O stretching modes, not present in the FTIR spectrum of the sample grown at 470 K, can be clearly observed (see Fig. 14b). Thus, in the presence of a controlled oxygen atmosphere, through which the plasma expands, films with a stoichiometry comparable to the one obtained in vacuum at temperatures as higher as 970 K can be grown, yet at temperature as low as 570 K. In order to further

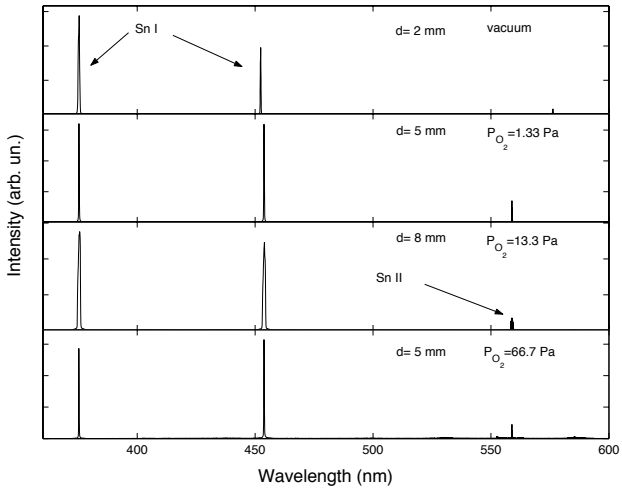

FIGURE 15. Time integrated optical emission spectra acquired in vacuum and for different P_{O2} values.

investigate the role played by the ambient pressure on film composition, a third set of samples was grown varying P_{O2} (from 0.13 up to 66.7 Pa), keeping constant the deposition temperature at the value of 470 K. In Fig. 14c the FTIR spectra of these samples and the compositional parameters x are reported. Upon increasing P_{O2}, x increases from 1.3 at P_{O2}=0.13 Pa up to 2.14 at P_{O2}=13.3 Pa, while x decreases down to 1.45 at P_{O2}=66.7Pa. The trend of x as a function of P_{O2} indicates that the relation between the oxygen content and its density in the chamber is a complex one. In fact, increasing P_{O2} up to 13.3 Pa, the oxygen content in the films decreases. This result indicates that the effects of the expanding plasma/gas interaction prevail over the trivial increase of oxygen gas density in the chamber. To further investigate about this aspect, optical emission spectroscopy and fast photography measurements were performed. In Fig. 15 are shown the time integrated spectra acquired in vacuum, for different P_{O2} values at a distance from the target at which the emission intensity was maximum.

In the spectra the emissions from Sn I (380.1 nm) and Sn II (579.9 nm) species are readily observed. Emission from neutral Sn species can be observed in all of the experimental conditions adopted while emission from ionized species could be observed only in the presence of P_{O2}.

In the same spectral region, time resolved optical emission measurements were performed. In Fig. 16 the time flight transient in vacuum, at 1.3,13.3 and 66.7 Pa are reported. These measurements allow to observe the variations of the Sn I and Sn II emission intensities as a function of the distance from the target surface. In vacuum there is no evidence of the emissions related to the ionized species while the emission intensity behavior from SnI species is characterized by a quick decrease as a function of the distance (see Fig. 16a). On the contrary, upon increasing P_{O2} (13.3 Pa), the Sn I intensity drastically decreases and, at the same time, the emission line at 579.9 nm related to the Sn II species become

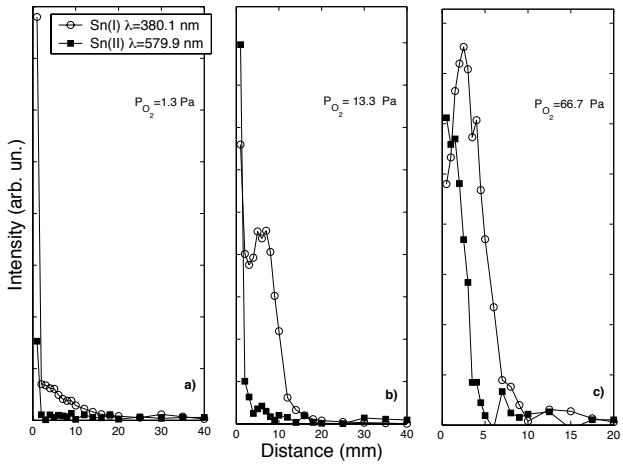

FIGURE 16. a) Intensity of Sn I and Sn II emissions as a function the observation distance from the target, for different oxygen pressure values.

evident (see Fig. 16b). With increasing P_{O2}, the emission intensities from Sn I species increased and a definite maximum can be observed. The maximum position shifts towards the target surface upon increasing oxygen pressure. It is located at about 6 mm from the target surface in the presence of P_{O2}=13.3Pa, while it shifts at about 5 mm in presence of P_{O2}=66.7 Pa. The increase of the emission intensities and the presence of the maximum are related to the increased interaction of the expanding plasma with background gas, as gas pressure is increased. The presence of a maximum value in the time integrated optical emission spectra is indicative of the formation of a shock wave, as discussed in the above paragraph, while the shift towards the target is due to plasma confinement as a consequence of gas-plasma interaction. On the contrary, in vacuum or at low P_{O2}, the interaction between the plasma and the background gas is limited and, in this case, the process behaves as a free expansion without shock wave formation. Concerning the intensity-distance behaviour for Sn II species, a well defined maximum is not evident at any distance value. This is consistent with the hypothesis that the ionized species are produced principally in the first stage of plasma formation near the target surface where the plasma density and energy are maximum. Sn ionization processes, thus, are more probably due to collisions between "free electrons" and Sn atoms, a process favored by the confinement of the plasma in the presence of a controlled oxygen atmosphere. CCD image of the emission of the expanding plasma for different delay times, both in vacuum and in the presence of different P_{O2}, were acquired. From the images the position of the plasma as a function of time was obtained. The plot of distance vs time, in dimensionless variables, is shown in Fig. 17. It is evident that, in vacuum and for P_{O2}=1.3 Pa, the atomic species reach the substrate placed at a distance of 40 mm from the target surface following a free expansion behavior. On the contrary, at the higher P_{O2}, the presence of the gas in the chamber induces a reduction of

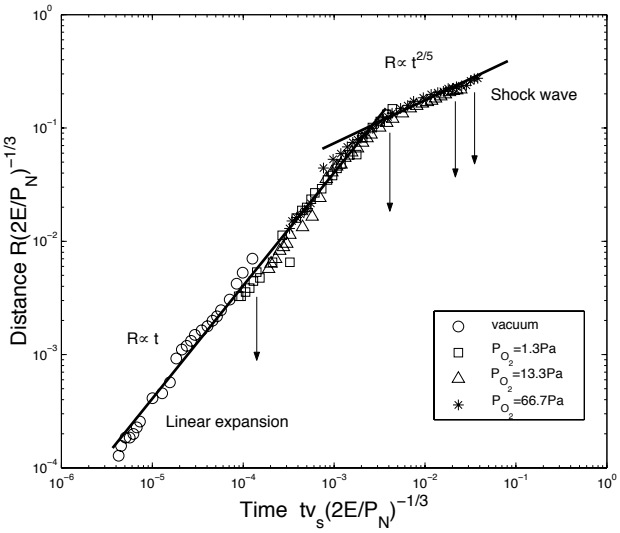

FIGURE 17. a) Variation of the distance R of the plasma front edge vs time in vacuum and for different P_{O2} values in terms of dimensionless variables.

the plasma expansion velocity with an evident confinement of the plasma at a distance of about 12 mm from the target.

The temperature in the contact region between the plasma and the background gas is so high to induce dissociation of gas molecules which react with the other species present in the plasma. Let's consider the following reaction:

$$Sn + O_2 \rightarrow SnO + O + \Delta E \tag{12}$$

the dissociation energy of an oxygen molecule is 5.16 eV, while the binding energy of SnO is 5.51 eV, then, the reaction is endothermic. An energy amount of about 0.4 eV can be easily provided in the internal region of the shock wave by the collisional processes. Thus, incorporation of oxygen in the films is favored not only by the presence of the oxygen gas in the deposition chamber, but also by the dynamics of the expanding plasma and its interaction with the background gas. In fact, in the presence of oxygen gas, but in absence of shock wave formation, it is not possible to grow nearly stoichiometric films. Nevertheless, when P_{O2} values are sufficient for shock wave formation, the reaction rate increases and the formation of SnO complexes occurs. The latter can be considered as the precursor for film growth. The fact that the dynamics of the expanding plasma is the fundamental process that can control oxygen content in the films is further confirmed by the fact that at P_{O2}=66.7 Pa, when oxygen density is maximum in the deposition chamber, oxygen content (x values) decreases from 2.1 down to 1.43. The absorption bands related to Sn-O and O-Sn-O vibrational modes are not well distinct but a unique broad band, typical of an amorphous material, results. The drastic worsening of the structural properties of the films

at such a high oxygen pressure cannot be related to the absence of SnO formation mechanism but to plasma confinement and to the drastic reduction of the energy of the species impinging on the substrates. In this respect, the role played by the plasma expansion dynamics is of paramount importance to determine the structural properties of the sample. Taking into account that the plasma dynamics is the result of different experimental parameters, such as gas pressure, its chemical nature and the initial energy of the plasma (i.e. the laser fluence), the analysis of film properties cannot be simply exploited in terms these parameters, but the plasma expansion regime must be taken into account.

5. Conclusion

Optical emission spectroscopy and fast photography measurements, performed during the deposition process of thin films of different materials, reveal that the dynamics of the laser generated plasma expansion plays a crucial role in determining the structural properties of the deposited materials. All the results were explained according to the Arnold et al. analytical model, which is able to describe the whole expansion process in terms of three temporal stages. The results, analyzed in terms of gas composition and pressure, can be summarized as follows:

- a shock-wave can develop when ablation is performed in the presence of a background gas. The shock wave formation depends on the plasma energy and gas pressure. In such a case, the chemical reaction rate, among the species present in the plasma and in the gas, increases as demonstrated by the study of the SiC target ablation at different partial pressures of nitrogen gas.
- while the development of a shock-wave undoubtedly favours chemical reactions, the observed increase of nitrogen atomic fraction in the SiC_xN_y films could be related to an increased availability of nitrogen molecules as the gas partial pressure was raised.

In order to separate the role played by plasma dynamics and by the density of the reactive gas, a series of experiments were performed during the expansion of a silicon plasma in a pure oxygen atmosphere and in a mixed oxygen/argon atmosphere at different partial pressures. The same approach was adopted growing CN_x thin films both in pure nitrogen and in a mixed nitrogen/argon atmosphere. A comparison between the influence of the dynamics of the expanding plasma on the composition and the structural properties of the two materials was made.

It was observed that:

- nearly stoichiometric SiO_2 was obtained in pure oxygen partial pressure only for pressure values greater than 6.5 Pa. When deposition took place in a mixed oxygen/argon atmosphere stoichiometric films were obtained in presence of just 1.3 Pa of oxygen. This behaviour is explained taking into account the formation of the shock wave, the only regime of the expanding plasma observed in the presence of a gaseous mixture.
- in the case of CN_x thin films, the emerged picture was complicated by the possibility of carbon atoms to assume different coordination and bonding configurations and by the fact that nitrogen content in the films seems to saturate to the value

of 0.3-0.4, irrespective of the deposition technique. In fact, the nitrogen content of the samples grown in the gaseous mixture, even though considering the total pressure at which they were deposited, is as low as that of the sample grown at 1.33 Pa in pure nitrogen gas. The decrease of the nitrogen content, above a certain nitrogen pressure, is related to the transition from free expansion to shock wave formation.

- the structure of the laser ablation deposited carbon-nitrogen thin films depends strongly on the dynamics of the expanding plasma (that is on gas composition and pressure) not simply on the nitrogen content as shown by Raman spectroscopy results. The growth of graphitic domains was observed when nitrogen content in the films decreases, as it happens for the sample grown at the highest partial pressure. This behaviour may be explained in terms of reduction of the kinetic energy of the depositing species when there is a transition from linear expansion to shock wave formation.
- Concerning SnO_x thin films, the results show that the deposition temperature and the oxygen partial pressure are two parameters which play a fundamental role in determining the oxygen content in the grown films. In the presence of oxygen partial pressures higher than 1.3Pa, it is possible to grow stoichiometric films at the deposition temperature of 470 K. Shock wave formation is considered the mechanism responsible for the increase of oxygen content in the films. Higher oxygen pressure induces formation of the shock wave, but also determines a reduction of the kinetic energy of the ablated species. So, the species, reaching the substrates, do not rearrange on the surfaces to minimize the presence of structural defects and/or to increase other reaction between the species. Then, the films grown at the highest oxygen pressure are substoichiometric and show poor structural properties.

The above outlined results are certainly representative of the PLD specific deposition conditions used. The influence, in different ways, of the dynamics of the expanding plasma (in vacuum, in pure background atmosphere, in gaseous mixture) on the grown film's structural properties was systematically investigated. The experimental results provide clear evidence of the strong correlation between film structural properties and plasma expansion dynamics well beyond any simple dependence on the overall reactive gas content.

References

[1] D.B. Chrisey, G.K. Hubler, D. Geoheagan, Pulsed Laser Deposition of Thin Films (Wiley, New York 1994) Chap.1 .
[2] D.B. Chrisey, G.K. Hubler, D. Geoheagan, Pulsed Laser Deposition of Thin Films (Wiley, New York 1994) Chap.5 .
[3] E. Fazio, E. Barletta, F. Barreca, F. Neri, S. Trusso, J.Vac.Sci.Technol.B **23**, 519-524 (2005).
[4] H.J. Dang, M.F. Zhou, Q.Z. Qin, Appl. Surf. Sci. **140**, 118 (1999).
[5] M. Okhoshi, T. Yoshitake, K. Tsushima, Appl. Phys. Lett. **64**, 3340 (1994).
[6] W.K.A. Kumuduni, Y. Nakayama, Y. Nakata, T. Okada, M. Maeda, J. Appl. Phys. **74**, 3340 (1993).
[7] J. Gonzalo, C.N. Afonso, I. Madariaga, *J. Appl. Phys.* **81** 951 (1997).
[8] P.E. Dyer, A. Issa, P.H. Key, Appl. Phys. Lett. **57**, 186 (1990).
[9] Y.B. Zel'dowich, Y.P. Raizer,*Physics of Shock Waves and High Temperature Hydrodynamic Phenomena*(Academic Press, New York 1966).
[10] L.D. Landau, E.M. Lifhitz, *Fluid Mechanics*, 2nd edn.(Pergamon Press, Oxford 1987).

[11] N. Arnold, J. Gruber, J. Heitz, Appl. Phys. A **69**, S87 (1999).
[12] F. Barreca, E. Barletta,E. Fazio,F. Neri, ,S. Trusso,B. Fazio, Radiation Effects and Defects in Solids **160**, 601-608 (2005).
[13] S. Trusso, E. Barletta, F. Barreca, F. Neri, Appl. Phys. A **79**, 1997-2005 (2004)
[14] S Wee, S.M. Park: Opt. Commun. **165**, 199 (1999).
[15] S. Acquaviva, M.L. De Giorgi, *Appl. Surf. Sci.* **186** 329 (2002).
[16] C. Vivien, M. Dinescu, P. Meheust, C. Boulmer-Leborgne, A.P. Caricato, J. Perriére, *Appl. Surf. Sci.* **127-129** 668 (1998).
[17] J. Hermann, C. Dutouquet, *J. Phys. D: Appl. Phys.* **32** 2707 (1999).
[18] Y. Yamagata, A. Sharma, J. Narayan, R.M. Mayo, J.W. Newman, K. Ebihara, *J. Appl. Phys.* **86** 4154 (1999).
[19] S.M. Park, K.H. Lee, *Appl. Surf. Sci.* **178** 37 (2001).
[20] A.A. Voevodin, J.G. Jones, J.S. Zabinski, L.Hultman, *J. Appl. Phys.* **92** 724 (2002).
[21] R.K. Thareja, A. Misra, S.R. Franklin, *Spectrochim. Acta Part B* **53** 1919 (1998).
[22] F. Fuso, L.N. Vyacheslavov, G. Masciarelli, E. Arimondo, *J. Appl. Phys.* **76** 8088 (1994).
[23] F.J. Gordillo-Vásquez, A. Perea, J.A. Chaos, J. Gonzalo, C.N. Afonso, *Appl. Phys. Lett.* **78** 7 (2000).
[24] E. Fazio, E. Barletta, F. Barreca, G. Mondio, F. Neri, S. Trusso, G. Messina and S. Santangelo Eds., Series Topics in Applied Physics 281-296 (2006).
[25] F. Barreca, E. Barletta, E. Fazio, F. Neri, S. Trusso, B. Fazio, Radiation Effects and Defects in Solids **160** 601-608 (2005).
[26] S. Trusso, E. Barletta, F. Barreca, E. Fazio, F. Neri, Laser and Particle Beams **23** 149-153 (2005).

[a] Enza Fazio, Francesco Barreca, Fortunato Neri
Università degli Studi di Messina
Dipartimento di Fisica della Materia e Tecnologie Fisiche Avanzate
Salita Sperone 31
98166 Messina, Italy
* **E-mail**: fneri@unime.it

[b] Barbara Fazio, Sebastiano Trusso
CNR-Istituto per i Processi Chimico-Fisici, Sezione di Messina
Salita Sperone, Contrada Papardo
98158 Messina, Italy

Presented: November 28, 2006
Published on line: September 26, 2007